UMYU Scientifica, Vol. 3 NO. 4, December 2024, Pp 094 – 107
https://doi.org/10.56919/usci.2434.009
ISSN: 2955 – 1145 (print); 2955 – 1153 (online)
A periodical of the Faculty of Natural and Applied Sciences, UMYU, Katsina

ORIGINAL RESEARCH ARTICLE

Fabrication and Characterization of Aluminum-Doped Nickel Oxide Thin Films for Optoelectronic Applications Using the SILAR Method

Okpechi-Kanayochkwu Uchechi Patricia[1], Elizabeth Chinyere Nwaokorongwu[2], Joseph U.[3], Akwuegbu Chinyere Ozorchi[4] and Ezere Uchechi[5]
[1,2,3,4,5]Department Of Physics, Micheal Okpara University of Agriculture Umudike, PMB 7267, Umuahia, Abia State Nigeria

ABSTRACT
The effect of varying the annealing time of %10 aluminium-doped Nickel Oxide thin film was studied to understand the possible effect on the optical, structural, and electrical properties of %10 aluminium-doped Nickel Oxide (ANO) for possible application. The thin films were deposited on glass substrates using the successive ionic layer adsorption reaction (SILAR) deposition technique. The samples formed were annealed at 300^{0}C, and the annealing time varied at 1.35 hrs., 1.45 hrs., 1.55 hrs., and 2 hrs, respectively. The deposited films were characterized to obtain the optical, electrical, and structural characteristics and the compositional constituent of the film using the double beam photo spectrometer, Four-Point Probe, Scanned electron Microscope, Energy Dispersion Spectroscopy, and X-ray Diffractometer. The films were observed to have low absorbance in the range of 0.1 to 0.01 and high % transmittance within the range of 80% - 98% in the visible region of the spectrum. The reflectance of the film was observed to decrease with an increase in annealing time in the range of 10% - 2.5%, all in the visible region of the spectrum. The crystallite size of the deposited films decreased with increased annealing time with the structural formation of simple cubic phase NiO thin film. SEM micrograph of the thin films reveals that an increase in annealing time improved the crystallinity of the films with the grain size evenly distributed. The EDS result of the deposited films revealed the presence of nickel, aluminum and Oxygen as the major constituent of the deposited films. The Ruther Ford Backscattering (RBS) analysis of the thickness of the films shows an increase in the thickness with an increase in annealing time. Clearer compositions of the films were also seen from the RBS analysis. Their electrical properties revealed that the films formed had low electrical resistivity and high conductivity, so they could be useful in making optoelectronics devices and corrosion resistance.

ARTICLE HISTORY
Received March 18, 2024
Accepted October 11, 2024
Published October 16, 2024

KEYWORDS
SILAR, doping, time variation, Nickel oxide, thin films

INTRODUCTION
Due to the rapid development of communities worldwide, the need for more technological breakthroughs in our present world has increased the search for new materials with unique properties that could be processed as thin films and integrated into energy storage and conversion based on their improved or modified properties for possible application. Thin film technology of metal oxides has had significant progress in various areas. It has impacted the development of various engineering, science, and technological materials like memory devices (Tuba *et al.*, 2019), light-emitting diodes, temperature sensors, and polymers, among various applications (Obaida *et al.*, 2022). One of the most important metal oxide thin films is the Nickel oxide (NiO) thin film, an essential p-type semiconductor due to its native p-type conductivity, good transmittance in the visible light range, and large work function. It has been widely studied as a promising material for possible applications in optoelectronic devices, electro-chromic display devices, gas sensors, p-type transparent conducting electrodes, thermoelectric devices, and magnetoresistance sensors (Gupta *et al.*, 2022). (Mohamed *et al.*, 2020). NiO with the NaCl-type structure is antiferromagnetic and has a wide band gap in the range of 3.6–4.0 eV (Osuwa *et al.*, 2012), Excellent durability and electrochemical stability (Tuba et al., 2019), low material cost, promising ion storage material in terms of cyclic stability, large span optical density and the possibility of manufacturing it by a variety of techniques

Correspondence: Okpechi-Kanayochkwu Uchechi Patricia. Department Of Physics, Micheal Okpara University of Agriculture Umudike, PMB 7267, Umuahia, Abia State Nigeria. ✉ chiemeriedalu@gmail.com. Phone Number: +234 806 342 6224

How to cite: Okpechi, K. U. P., Nwaokorongwu, E. C., Joseph, U., Akwuegwu, C. O., & Ezere, U. (2024). Fabrication and Characterization of Aluminum-Doped Nickel Oxide Thin Films for Optoelectronic Applications using the SILAR Method. *UMYU Scientifica*, 3(4), 94 – 107. https://doi.org/10.56919/usci.2434.009

are the other attracting features of NiO thin film.(Obaida, *et al,* 2022). Nickel Oxide is a low-cost, abundant semiconductor and can be created at the scale needed to meet widespread demand. The synthesis and studies of nanosized Metal oxide semiconducting materials have been intensively pursued in recent years not only because of their characterization interest but also for their interesting catalytic, thermal, magnetic, electrical, and optical properties and the variety of applications related to them (Tuba *et al.*, 2019). In recent years, various techniques have been employed in the deposition of nanostructured transition metal oxides thin films: methods such as thermal evaporation, spray pyrolysis (Obaida *et al.,* 2022), chemical bath deposition (solution growth techniques) (Osuwa *et al.*, 2012, Pathan 2002), chemical vapour deposition, etc. (Yun *et al.*, 2019), Spin coating (Kumar et al., 2022), Pulser-laser ablation (Mohammed *et al.*, 2020), sol-gel method (Zayim et al., 2008). Nid *et al.*, (2021) studied Al-doped NiO thin film using solar spray pyrolysis technique, deposited at different atomic percentage ratios and observed the structural formation of (NiO) phase under a cubic crystalline structure with optical transmission in the visible region of about 65%, a decrease in optical band gap from 3.69 to 3.64 eV, the films were found to exhibit high conductivity, its good transparency and high electrical conductivity makes them good material for optoelectronic device. Yahya *et al.* (2019), studied the structural properties of AL-doped Nickel oxide and observed a polycrystallinity phase with a cubic crystalline structure. Anusha *et al.,* 2023, deposited AL-doped Nickel oxide by dip coating at different temperatures. The optical properties indicated high transmittance in the visible region of the spectrum with an increase in the optical band gap from 3.42 eV to 3.38eV. The Successive Ionic Layer Adsorption Reaction (SILAR) method is used in this work. It synthesized 10%Aluminium doped Nickel Oxide thin film annealed at 3000C. The time of annealing varied to study the effect of time variation on the thin film's electrical, structural, optical, and elemental composition to ascertain its properties and possible applications. NiO was chosen as the host lattice, while Al was a dopant for the film.

MATERIALS AND METHODS

NiO thin films were synthesized on a glass substrate at room temperature using the Successive Ionic Layer adsorption and Reaction [SILAR] method. $NiCl_2.6H_2O$ was used as a source of the Ni^{2+} ion, while NaOH is the source of the hydroxide ion OH^{-1} which was converted to the oxide after annealing the ions. $AlCl_2$ was used as the Al (dopant ion) source, while NH_4OH was used as the complexing agent. The substrates were immersed into a complex solution bath containing 40g of 0.6M $NiCl_2.6H_2O$ with 10% AlCl2 introduced as dopant at 55∘C temperature. Distilled water was used as the ion exchange water. 37.2g of 0.5m of NaOH also was used as a source of OH^-. The pH value of the solution was also set at 8.0. An immersion of the substrate into the solution for (20secs) followed by immersion in ion exchange water for about 5secs for hydrogenation, followed by immersion into NaOH for another 20secs and then to ion exchange water for 5secs and back to the complex solution. The cycle was repeated for 20 cycles to achieve the desired result. The deposited films were annealed at 300°C, varying the annealing time at 1.35hr, 1.45hr, 1.55hr, and 2hrs to study the effect of time on annealing.

DESCRIPTION OF DEPOSITION TECHNIQUE

The SILAR method is adopted on the principle of adsorption and reaction of the ions from the solutions and rinsing between every immersion with distilled water to avoid homogeneous precipitation in the solution. Figure 1 shows the schematic representation of the SILAR method

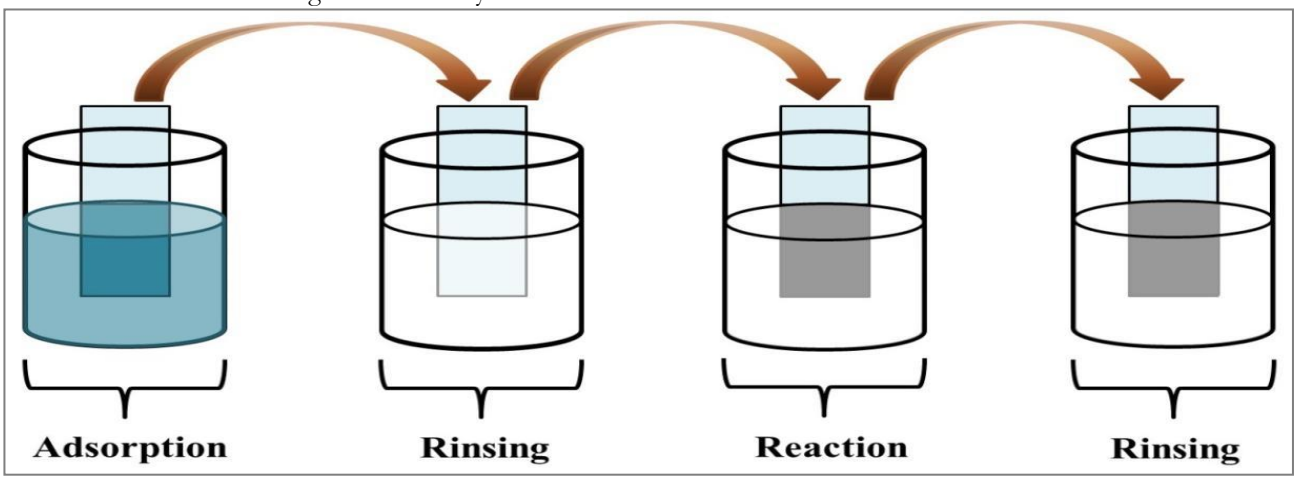

Figure 1: **Schematic representation of SILAR method [Onwuemeka et al., 2019]**

Mathematical method used:

The structural properties were studied using X-ray diffraction (XRD), a basic method for determining the crystalline structure of samples. The analysis of XRD is usually based on the principles of constructive and destructive interferences of monochromatic X-rays and a crystalline sample. The X-rays are produced by a cathode ray tube, sieved to produce monochromatic radiation, collimated to concentrate, and focused toward the sample. The interaction of the incident rays with the

sample produces constructive interference (and a diffracted ray) when conditions satisfy Bragg's law.

$$n\lambda = 2d \sin\theta \quad (1)$$

Where θ is the angle of diffraction between the primary X-ray beam (with λ as wavelength),

d is the interplanar spacing;

and n is an integer.

This law relates the wavelength of electromagnetic radiation to the diffraction angle and the lattice spacing in a crystalline sample. X-ray diffractometer modeled GBC Enhanced Mini Material Analyzer (EMMA) was used in analyzing the material. It gives information about the nature and structure of the doped thin films of AlMnO. The resolution of Scherer's equation obtained the crystallite size:

$$D(hkl) = \frac{k\lambda}{B\cos\theta} \quad (2)$$

Where:

D(*hkl*): The average crystallite or particle size in the direction of plane (hkl) (nm)

λ: The X-ray wavelength (nm) Where λ is the wavelength of Cu-K radiation (λ =1.54060 0A)

K: A dimensionless shape factor (*K* = 0.94)

B: Full Width at Half Maximum (FWHM) of the diffraction peak (rad)

θ: Bragg diffraction angle (deg)

The lattice parameter, which refers to the physical dimension of unit cells in a crystal lattice with three lattice constants for three-dimensional lattices denoted by a b, c for the thin films, was calculated for different phases of the materials deposited.

For the cubic phase, the lattice constant was calculated from

$$\frac{1}{d^2} = \frac{h^2+k^2+l^2}{a} \quad (3)$$

Where 'd' is the interplanar distance, and hkl is the Miller indices.

The microstrain was calculated using:

$$\varepsilon = \frac{a\cos\theta}{4} \quad (4)$$

The dislocation density (d) was determined using.

$$\boldsymbol{\partial} = \frac{\mathbf{1}}{\boldsymbol{D^2}} \quad (5)$$

where 'D' is the crystallite size

The volume for simple cubic was calculated from

$$V = a^3 \quad (6)$$

Optical Measurements

The optical properties of the thin films are defined by the interaction between electromagnetic radiation (light) and the material, including absorption, diffraction, polarization, reflection, refraction, and scattering effects. The measurements are simple as long as a satisfactory spectroscopic apparatus is available in the wavelength region of interest. In this work, the optical performances of the thin films, which essentially consist of absorbance, transmittance, and reflectance, were studied using a UV1-1800 series double-beam spectrophotometer. The absorbance of the deposited films was measured using a UV-spectrophotometer and occurred in the electromagnetic spectrum's spectral range of 300nm-900nm. Other spectral/Optical parameters, such as transmittance, reflectance, etc, were estimated using appropriate mathematical formulas.

Transmittance

The values of absorbance were converted to transmittance using:

$$\%T = \text{antilog}(2 - \text{absorbance}) \quad (7)$$

Reflectance (R)

The reflectance was estimated using the equation (Akpu et al., 2022).

$$1 = A + T + R \quad (8)$$

Where A is the absorbance, T is the transmittance, and R is the reflectance of the deposited films.

For normalization, equation 8

becomes

$$R = 1 - (T + R) \quad (9)$$

Absorption coefficient (α)

Absorption coefficient is the fractional decrease in radiation intensity per unit increase in distance (Akpu et al., 2022). When a beam of electromagnetic radiation $\mathbf{I_o}$ is incident on a thin film surface, then

$$I = I_o e^{-\alpha t} \quad (10)$$

Where t is the distance traveled by the radiation, and I is the radiation intensity of thickness.

But equation 10 can be written as

$$I/I_o = e^{\alpha t} \quad (11)$$

From equation 11, it becomes

$$1/T = e^{\alpha t} \quad (12)$$

Taking the natural log of the equation 12 becomes

$$\text{Ln}\,(1/T) = \alpha t \quad (13)$$

For a unit distance, equation 13 becomes

$$\text{Ln}(1/T)=\alpha \quad (14)$$

Therefore, the absorption coefficient is;

$$A = \text{LN}\ (1/T) \quad (15)$$

Equation 15 was used to deduce the absorption coefficient of the thin film.

Optical energy band gap (E_g)

The relationship between the absorption coefficient (α) and incident photon energy (hv) can be determined using well-known Tauck's relations (Ibe and Mgbenu, 2008).

$$(\alpha h\nu) = A\ (h\nu - E_g)^n \quad (16)$$

Where v is the frequency of the incident photon, h is Planck's constant, A is a constant, E_g is the optical band gap, and n is the transition type.

It has been established that the measured absorption data fits well with the equation (Yang, et al., 2022) for n = 1/2 for directly allowed band gap semiconductors.

$$(\alpha h\nu) = A\ (h\nu - Eg)^{1/2} \quad (17)$$

Taking the square of both sides of equation 17, we have

$$(\alpha h\nu)^2 = A(h\nu - E_g) \quad (18)$$

Hence, the graph of $(\alpha h\nu)^2$ against $h\nu$ was plotted, and values of optical band gap energies E_g were obtained from extrapolating the straight portion of the graphs on the photon energy ($h\nu$) axis at $(\alpha h\nu)^2 = 0$.

Extinction coefficient (k)

The extinction coefficient (k) of the films was determined using the equation for semiconductors and insulators (Akpu et al., 2022)

$$K = \alpha\lambda/4\pi \quad (19)$$

Where α is the absorption coefficient of the thin film, and λ is the wavelength of the incident electromagnetic radiation.

Refractive index (n)

The relationship between the index of refraction (n_s) and the film reflectance (R) was used to estimate the refractive index (Obaida *et al.*, 2022);

$$R = (n_s - 1)^2 / (n_s + 1)^2 \quad (20)$$

Equation 20 is simplified

$$n = (1 + (R)^{1/2}) / (1 - (R)^{1/2}) \quad (21)$$

Dielectric constant (ε)

The complex dielectric constant (ε) is given by;

$$\varepsilon = \varepsilon_r + \varepsilon_i = (n + jk)^2 \quad (22)$$

Where ε_r = real part, ε_i = imaginary part, n =refractive index, and k = extinction coefficient.

Expanding equation 22, we obtain;

$$\varepsilon = \varepsilon_r + \varepsilon_i = (n^2 - k^2) + 2njk$$

Equating the real and imaginary parts of the equation (Obaida *et al.*, 2022), we have that,

$$\varepsilon_r = (n^2 - k^2) \text{ (The real part)} \quad (23)$$

$$\varepsilon_i = 2nk \quad \text{(The imaginary part)} \quad (24)$$

Optical conductivity (σ_o)

The optical conductivity was estimated by the equation (Obaida *et al.*, 2022);

$$\sigma_o = \alpha nc/4\pi \quad (25)$$

Where c is the speed of light in vacuum, α is the absorption coefficient, and n is the film's refraction index.

RESULTS AND DISCUSSION

Optical properties of (Aluminum Doped Nickel Oxide) ANO thin film

Figure 2 shows the absorbance of all the films, which were generally low in the 700nm–800nm region measured along the visible–infrared region of the spectrum. Figure 3 shows the transmittance of the films, which followed a particular pattern and were relatively high. It is observed from the graph that aluminum doping and increased variation of the annealing time increased the %transmittance of the films from 80% to 98% in the visible–infrared region of the spectrum, thereby making the material suitable for smart windows and materials for the construction of poultry roofs and walls, protecting the birds from UV radiation which is dangerous to human and animal health (Osuwa *et al.*, 2012). Figure 4 shows that reflectance was at 3 – 11 % reflectance but rises uniformly to 20 % reflectance with broad peaks at 760 nm - 800 nm of the wavelength of the spectrum. The broad reflectance peaks seen could be attributed to the number of vibrational energy levels available at that particular electronic energy level, and transition in different vibrational levels could result in sharp peak broadening. The result shows that since the reflectance of the samples is low, the films are good materials for reducing reflection losses because of their high transmittance and low absorbance. (Osuwa *et al.*, 2012). Figure 5 is the plot of the optical conductivity, which reveals high optical conduction in the visible region of the spectrum.

Figure 6 shows the plot of $(\alpha hv)^2$ versus photon energy, explaining the optical band gap of the films to be 1.59 eV for the un-annealed but decreases to 1.56 eV for the film for 1.35mins, and 1.58eV for film annealed for 2hrs. The band-gap energy of semiconductors tends to decrease with increasing temperature. When temperature increases, the amplitude of atomic vibrations increases, leading to larger interatomic spacing (Akpu et al., 2022). In this work, Doping reduced the band gap of NiO, which, according to the literature, is between 3.6 to 4.0eV, but was reduced

to 1.59. This could be as a result of the deposition method used.

Moreover, annealing time slightly affected the film band gap as the annealed films were observed to drop from 1.59 eV to 1.58eV and 1.56eV. This could be because the crystal lattice expands and the interatomic bonds are weakened (Zayim et al., 2008). Figures 9 and 10 show that the real dielectric constant has higher values than the imaginary dielectric constant. The result is consistent with the findings of Ugwu and Onah, (2007), and Nid *et al.*, (2021), This makes the ANO thin films good materials for microelectronics.

Figure 7 is the plot of the absorption coefficient of the films, and it was observed to be generally low; an increase in the annealing time increased the conductivity of the materials. The spectral dependence of the absorption coefficient affects the solar conversion efficiency (Ezeokoye et al., 2003). Thus, the low absorption coefficient indicates that light is poorly absorbed. Thus thin films of ANO may not be good materials in solar energy conversion applications (As solar energy collectors).

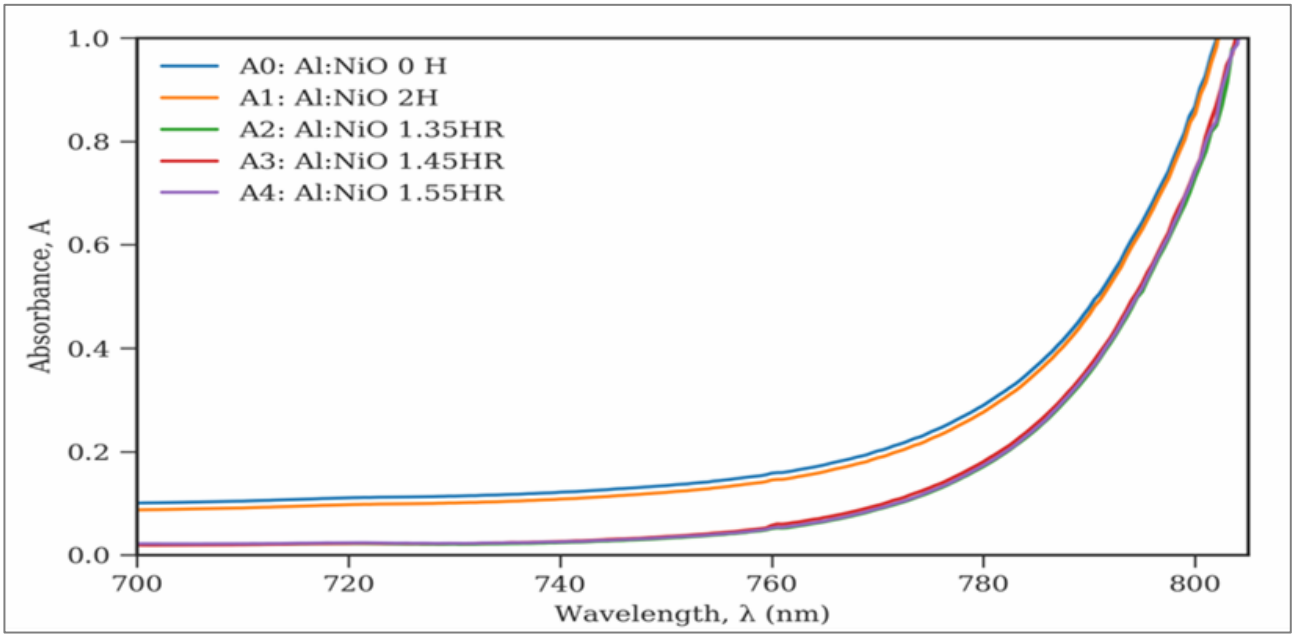

Figure 2: Plots of absorbance versus wavelength of ANO thin film annealed at varying time

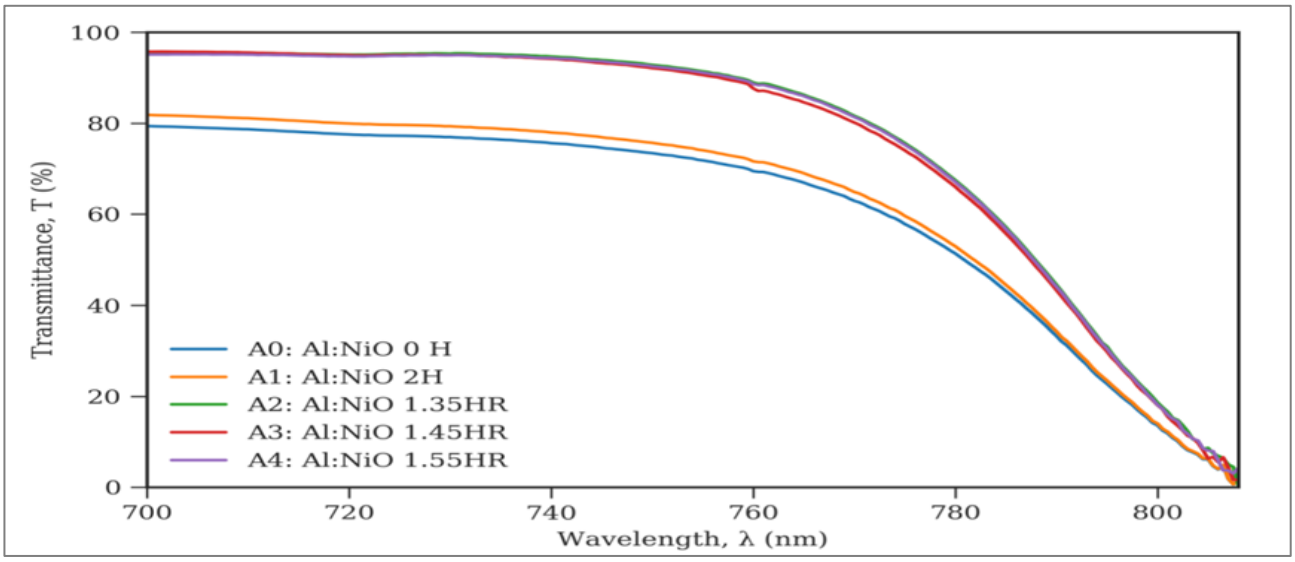

Figure 3: Plots of %Transmittance versus wavelength of ANO thin film annealed at varying time

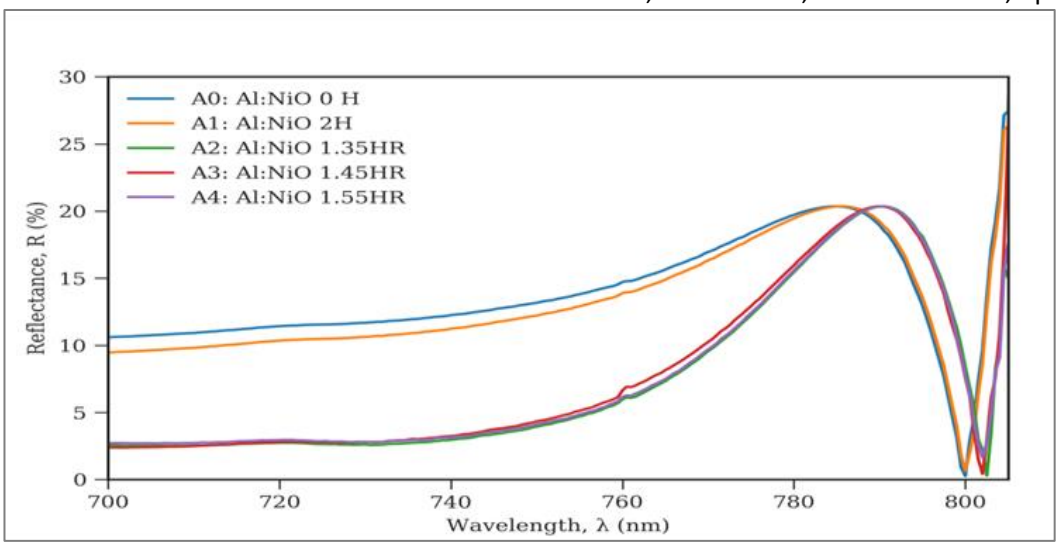

Figure 4: Plots of Reflectance versus wavelength of ANO thin film annealed at varying time

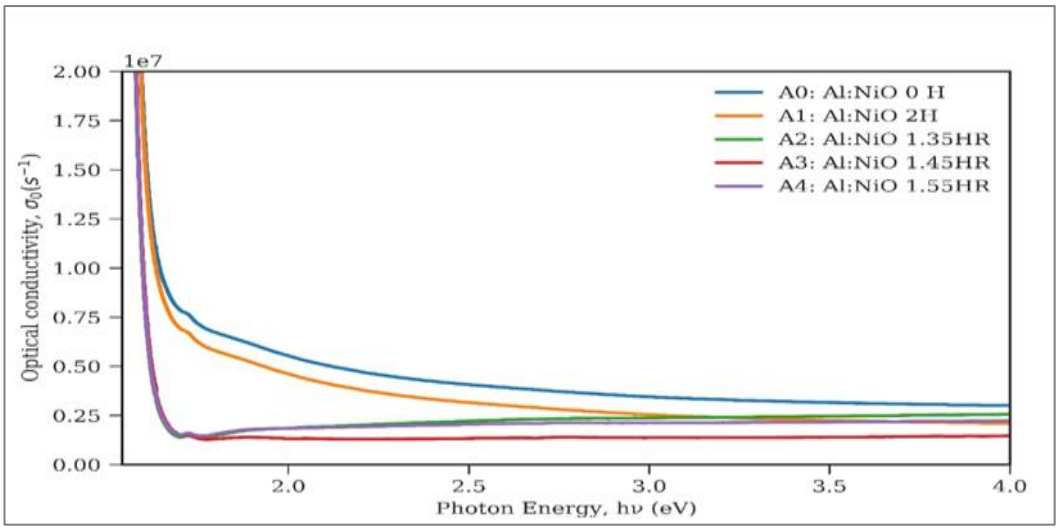

Figure 5: Plots of optical conductivity versus photon energy of ANO thin film annealed at varying time

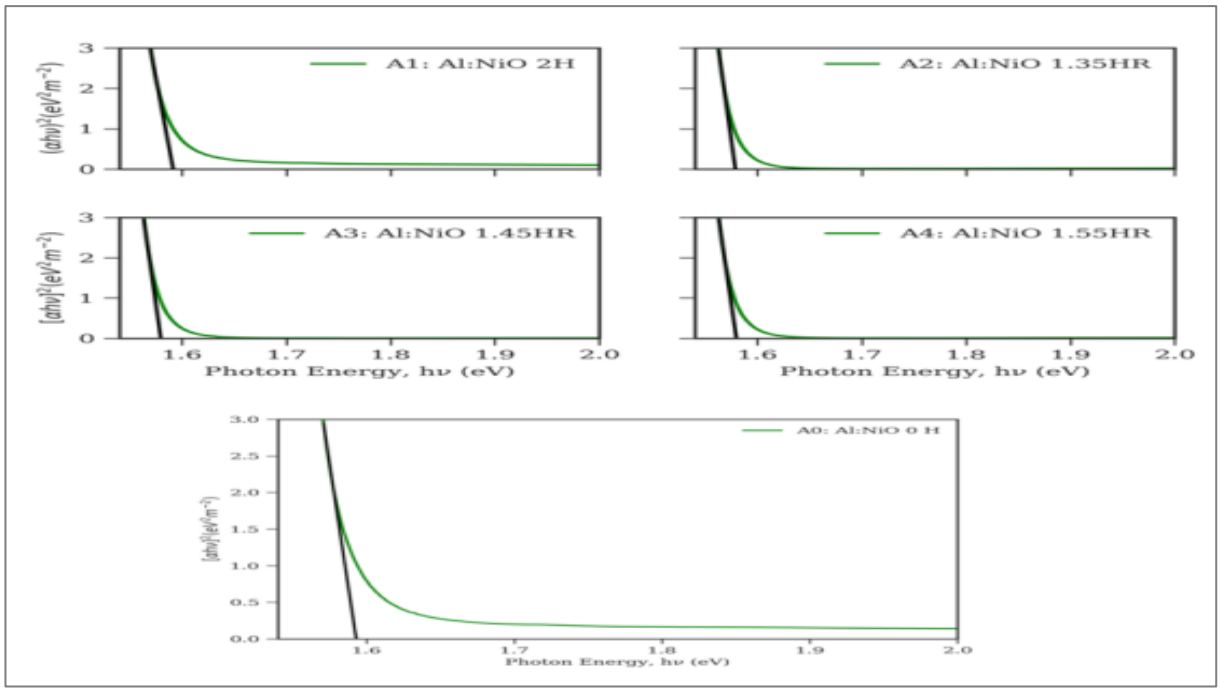

Figure 6: Plots of(αhv)²Versus Photon Energy of ANO thin film annealed at varying time

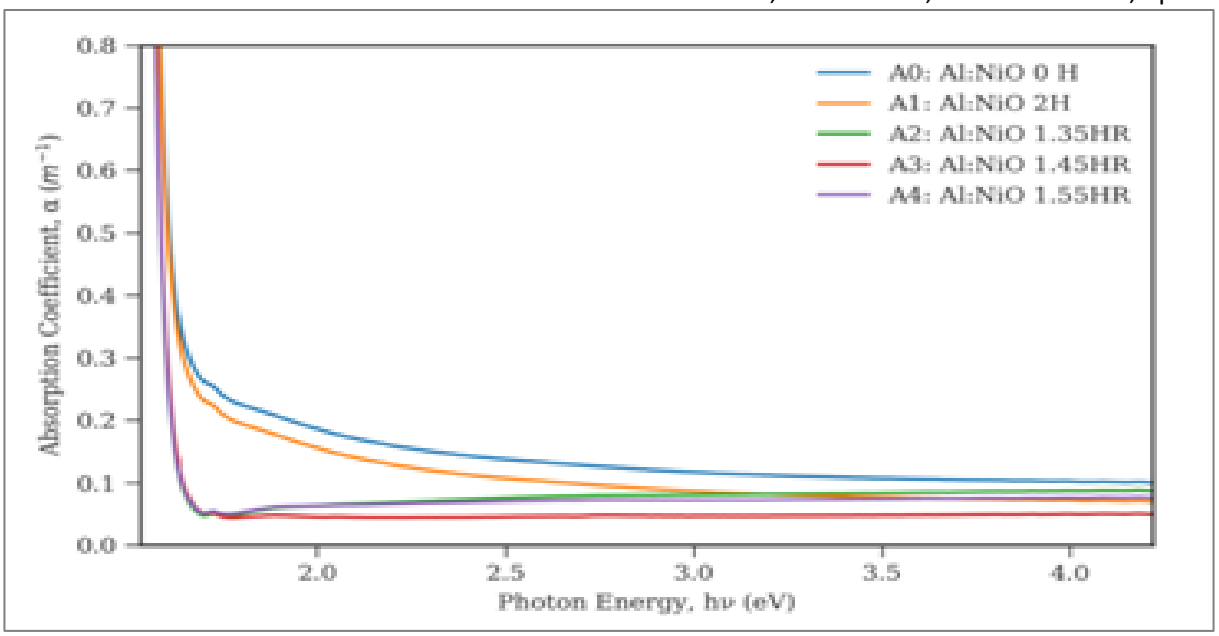

Figure 7: Plots of absorption coefficient versus Photon Energy of ANO Thin Annealed at Varying Time

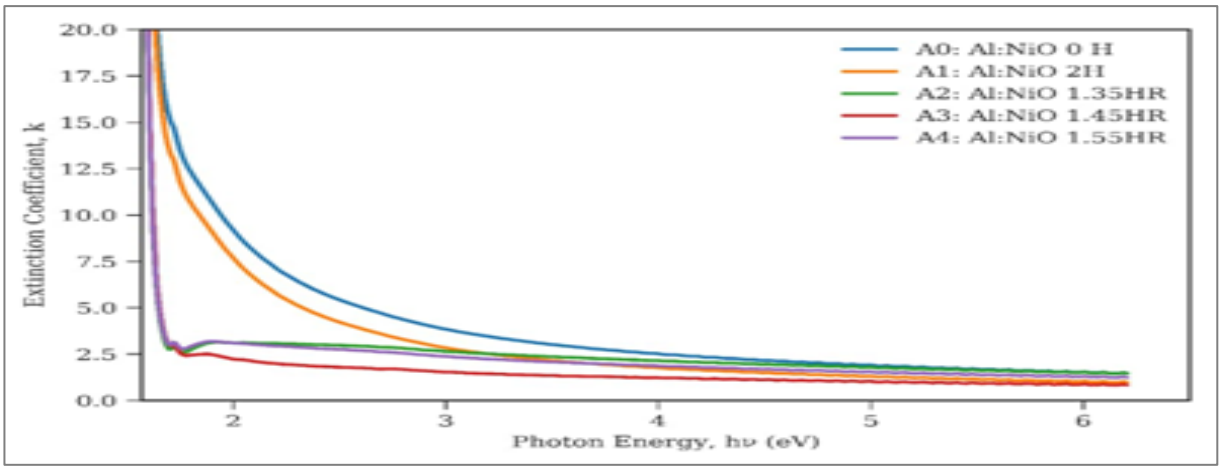

Figure 8: Plots of Extinction Coefficient versus Photon Energy of ANO Thin Film Annealed at Varying Time

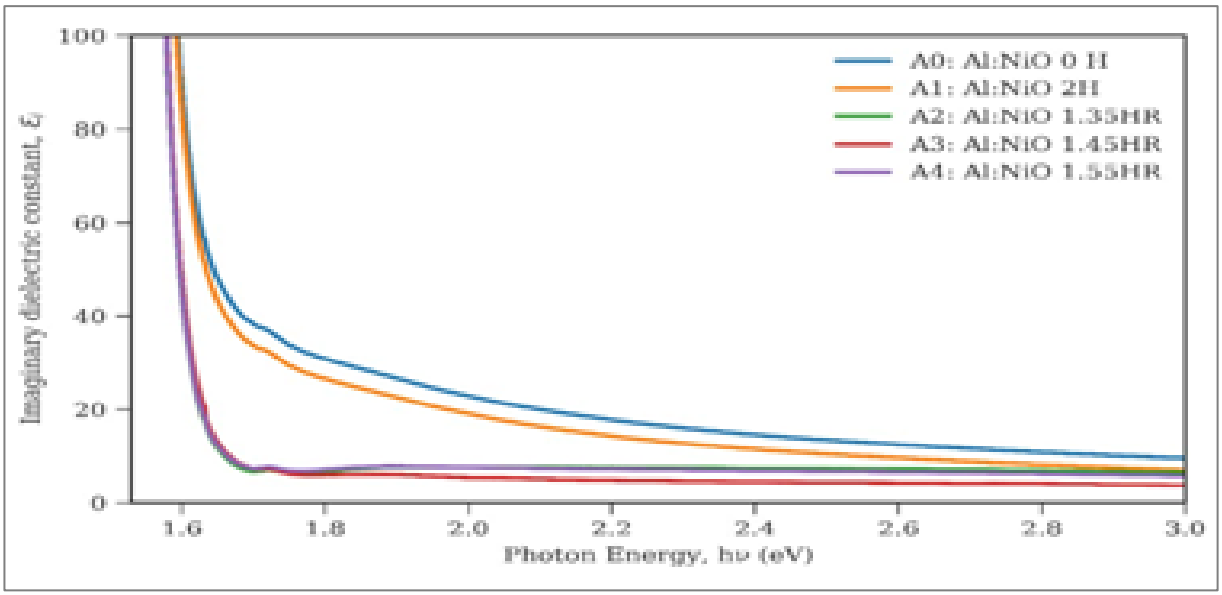

Figure 9: Plots of Imaginary Dielectric Constant versus Photon Energy of ANO Thin Film Annealed at Varying Time

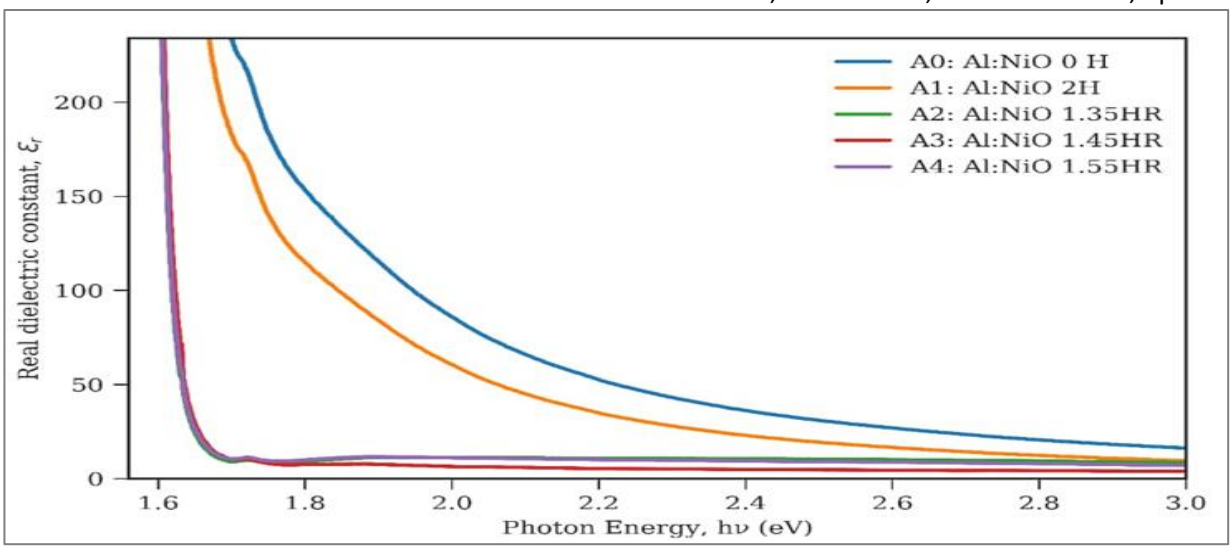

Figure 10: Plots of real dielectric constant versus photon energy of ANO thin film annealed at varying time

Structural properties of ANO thin films

Figures 11 and 12 show the XRD patterns obtained from ANO thin films. A simple cubic structure of the ANO thin films conformed with JCPDS card no 71-1123 and 46- 1212 reference patterns, respectively. Also, Yahya *et al.*, (2019) observed a polycrystalline phase with a cubic Crystallinity structure of Al-doped NiO thin film. The X-ray diffraction peaks at 31.3°,34.7°,38.9°, 42.6º, 45.0º,56.3º, 63.3°, 75.1° correspond to the cubic phase of NiO, Ni_2O_3 and are assigned to the (0 0 2), (110),(111),(2 0 0), (2 0 2), (2 2 0) and (311) crystallographic planes, respectively. The peak of 46.9º is the diffraction peak of Al and is assigned to the (012) crystallographic plane. The crystallite size increases with the film's thickness and annealing time. For films annealed for 2hrs, the x-ray diffraction peaks were at ,33.4º, 37.3º,40.4º, 42.6º, 45.2°,56.3°,63.3º,75.4º corresponding to the simple cubic phase of NiO_2 and are assigned to the (0 0 2),(110),(111),(200),(202),(220),and (311) crystallographic planes. The aluminum peak was found at 46.9°with a plane of (012). The average crystallite size was about 3.6 for film annealed for 1.35mins and 3.4 for film annealed for 2hrs. This is in line with the results of Boukachem *et al.* (2014), where the crystallite size increased with an increase in temperature. Other structural properties of ANO thin film, including lattice parameter dislocation density, volume, microstrain, and crystallite size, were calculated and are in Table 1. It was observed that the ANO thin films' lattice constant, dislocation density, microstrain, unit volume, and crystallite size increased with an increase in annealing time. Moreover, Figure 13 and 14 show the SEM micrograph of the Aluminum Nickel oxide thin film ANO, which indicates that the films were evenly distributed with rough film surface. Obaida *et al.*, (2022), in their study of NiO thin film, used spray pyrolysis to synthesize NiO films and observed that at high temperatures, NiO films were polycrystalline with Cubic phase and Nano size scale with SEM micrograph revealing rough film surface.

Film composition and thickness

The Rutherford backscattering was used to ascertain the film's composition and thickness. Figures 15, 16, 17, 18, and 19 show the ANO thin films' peaks at different annealing times. The film thickness increased with the increase in annealing time with variations in Aluminum and Nickel oxide composition despite equal doping concentration during preparations. Nickel oxide and aluminum were also represented in good proportion.

***Electrical property*:**

Figure 20 shows the plot of resistivity versus thickness of the **ANO** thin films in the range of 0.19 **Ω**m – 0.25 **Ω**m and increased with increased thickness. This is in line with the work of Haunsbavi *et al.*, 2022, where increased thickness increases the film's resistivity. Figure 19 shows the plot of resistivity with time of annealing. It shows that resistivity increased with an increase in time variation of annealing. According to the work of Osuwa and Uwaezi, (2012) on annealed NiS_2, according to Ibe and Mgbenu, (1997), resistivity increased with an increase in the annealing temperature of NiS_2 thin films annealed at different temperatures. Figure 21 shows the plot of conductivity against film thickness. It shows that conductivity increased randomly with the decrease in film thickness in the 5.25 S/m - 3.18 S/m range. Figure 22 shows the plot of resistivity against annealing time, which increased with an increase in annealing time. Figure 23 shows the plot of conductivity against time. It is observed that conductivity decreased with increased annealing time.

Table 1: Structural properties of ANO thin films

time	Lattice constant a	Dislocation density	Microstrain	Unit cell volume	Crystallite size
1.35 hrs.	3.0214	0.5985	16.7207	47.493	2.2287
2 hrs.	3.4034	0.7969	16.9208	39.422	0.1486

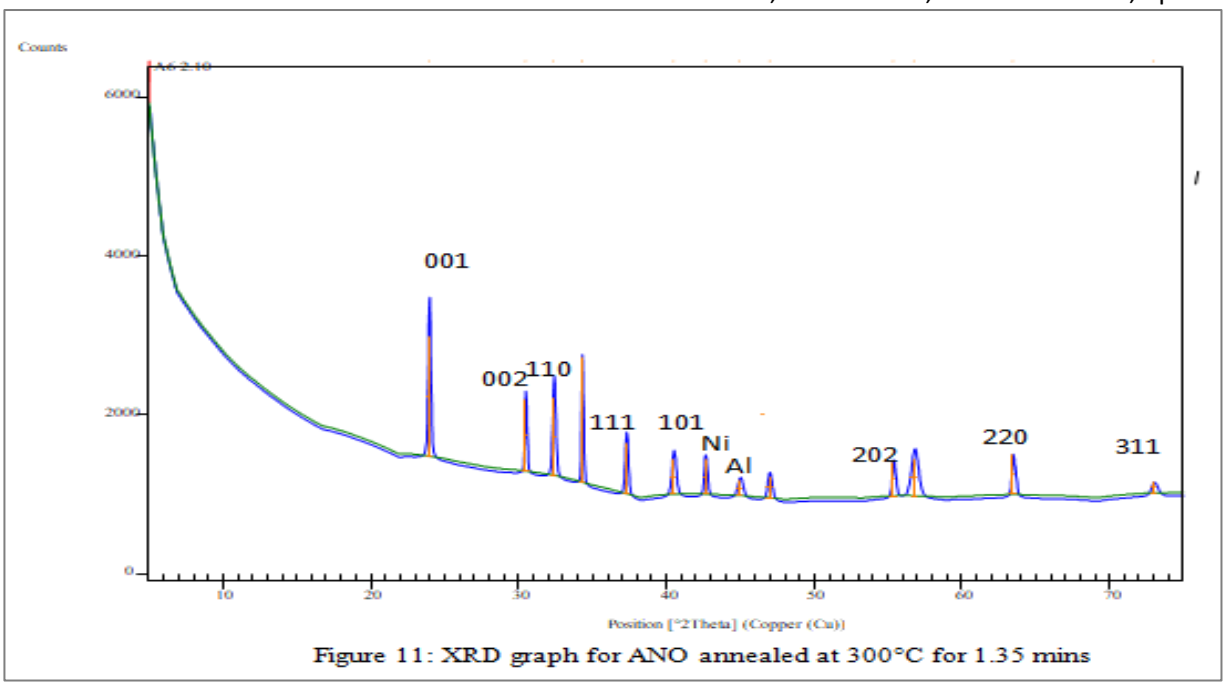

Figure 11: XRD graph for ANO annealed at 300°C for 1.35 mins

Figure 11: XRD Graph for ANO Annealed at 300^{0}C for 1.35 Minutes

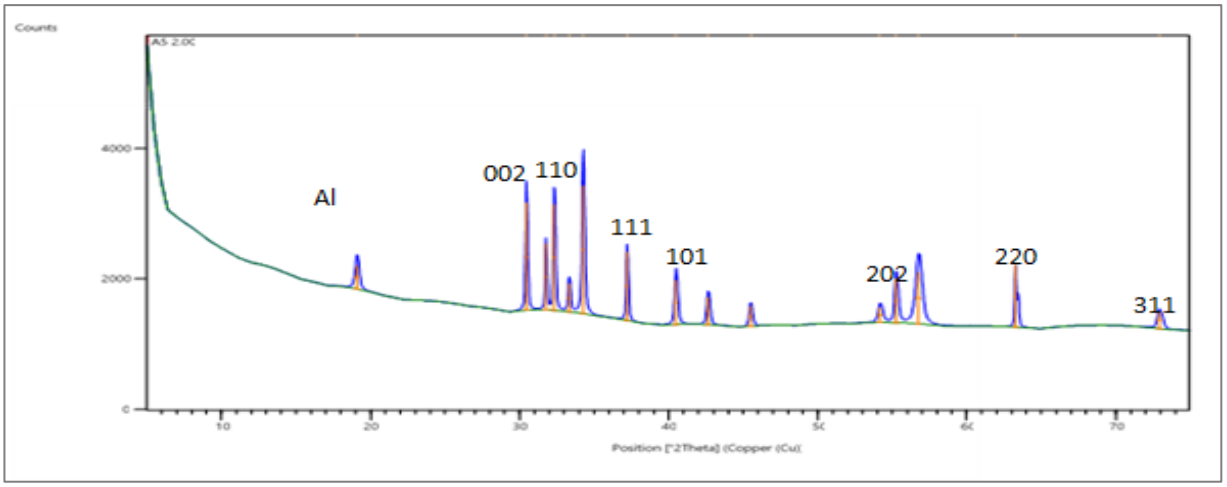

Figure 12: XRD Graph for ANO Annealed at 300^{0}C for 2 Hours

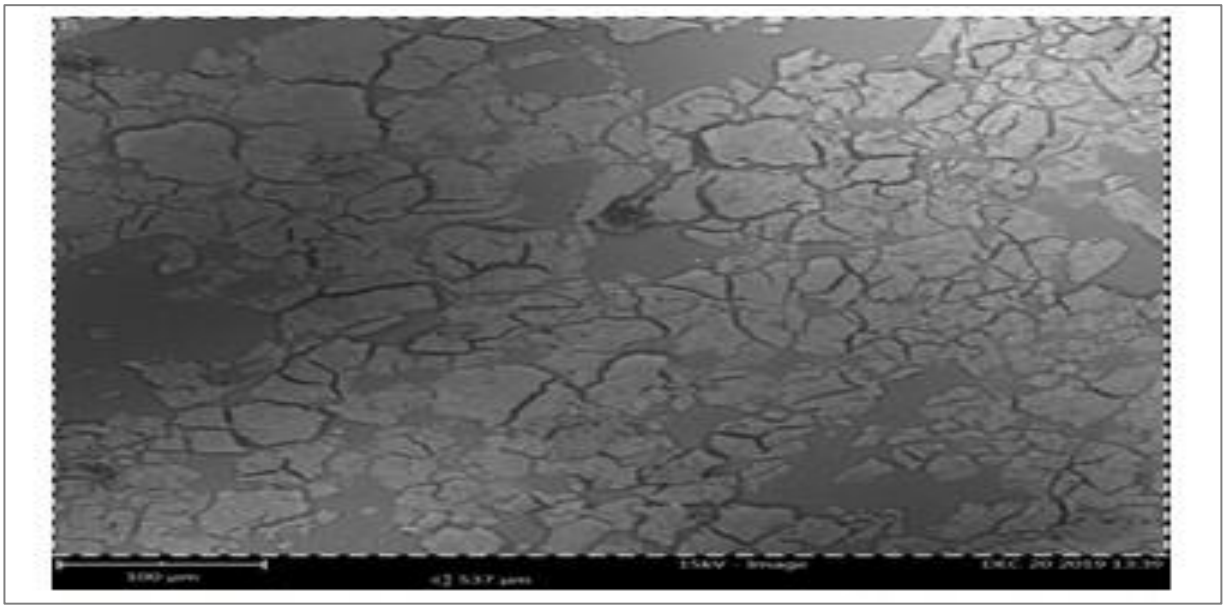

Figure 13: SEM Micrograph for ANO Annealed for 1.35 Minutes

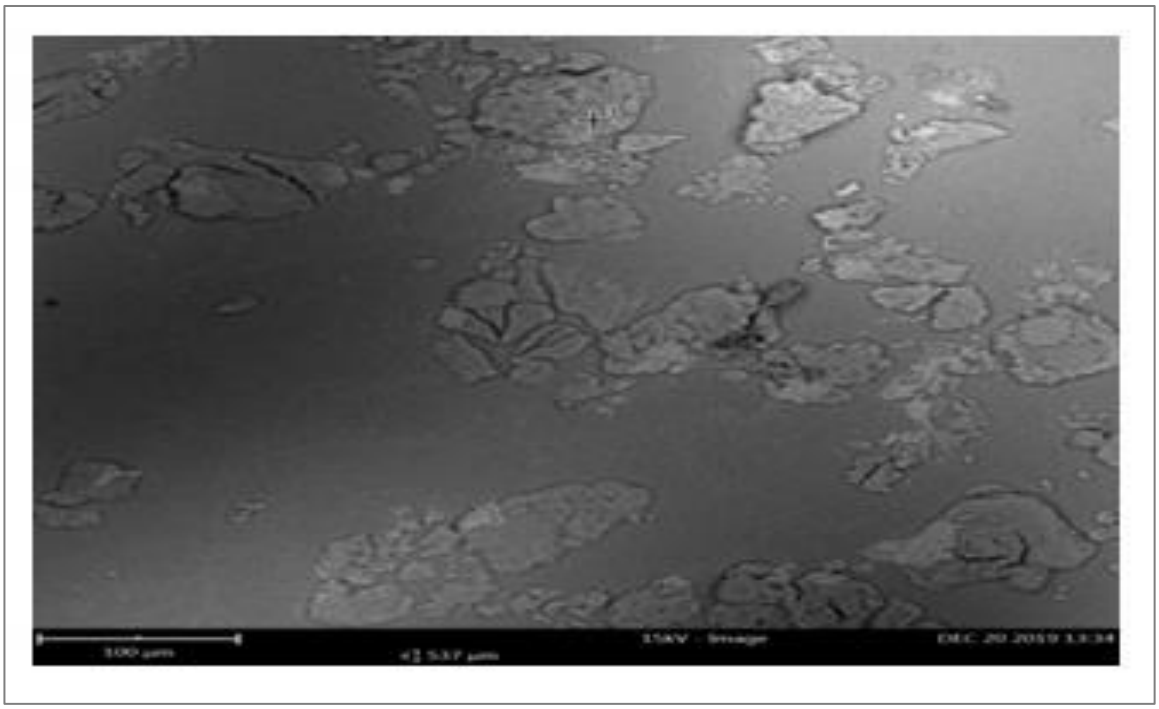

Figure 14: SEM Micrograph for ANO Annealed for 2 hours

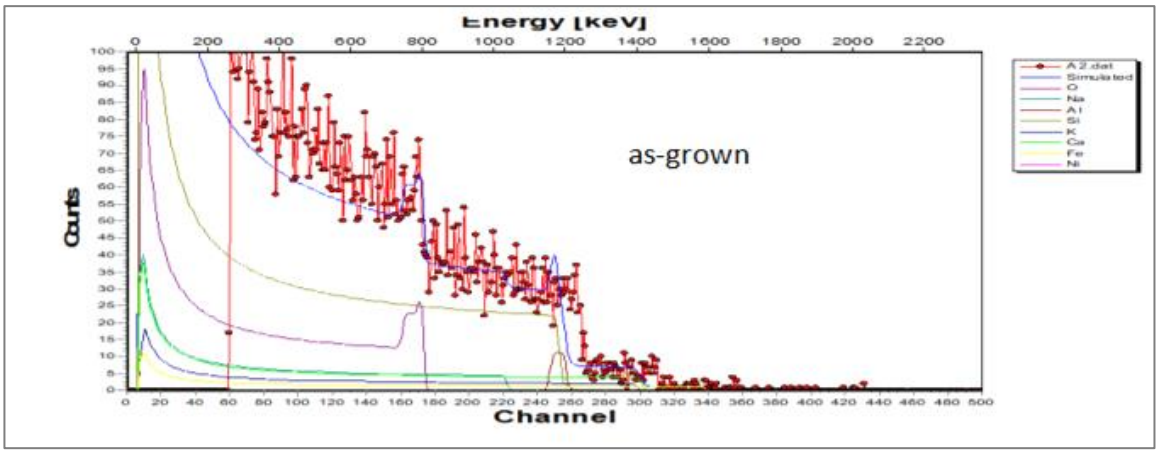

LAYER 1: THICKNESS: 148nm Compo: Ni = 15.69%, Al = 0.5 %, O = 84.31%
LAYER 2: THICKNESS: 5000 nm Compo: A glass substrate

Figure 15: RBS Analysis for ANO annealed for 300°C for As Grown

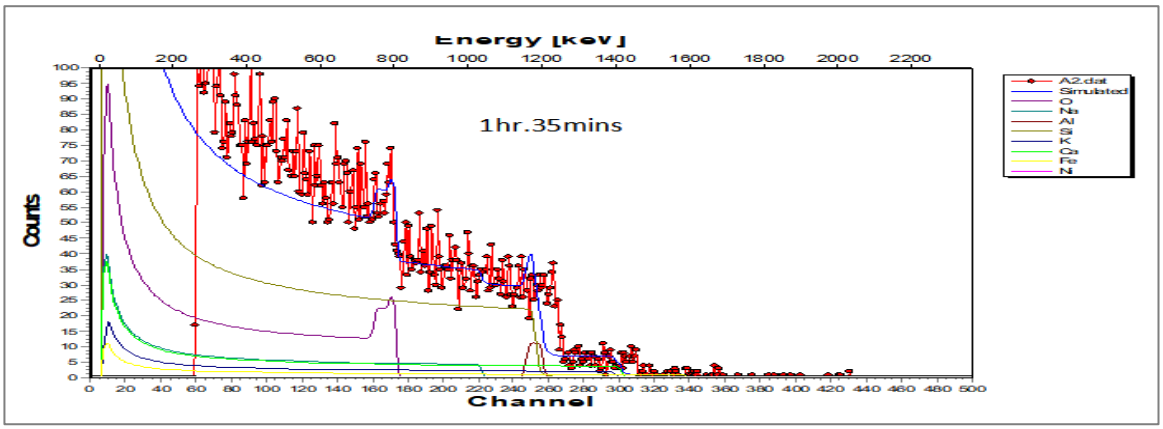

LAYER 1: THICKNESS: 150 nm Compo: Ni = 4.47%, Al = 8.98 %, O = 87.55%
LAYER 2: THICKNESS: 5000.0 nm Compo: Si = 35.19%, O = 51.09.81%, Ca = 2.16%, Al = 0.02%, K = 1.41% and Fe = 0.39%

Figure 16: RBS Analysis for ANO annealed for 300°C for 1.35mins

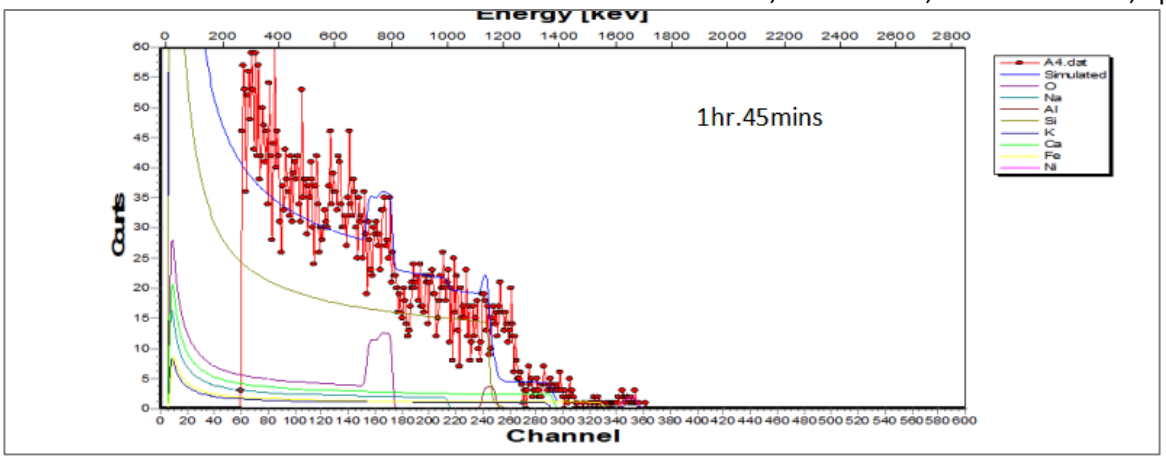

LAYER 1: THICKNESS: 168.0 nm Compo: Ni = 1.32%, Al = 15.14%, O = 83.55%
LAYER 2: THICKNESS: 5000.0 nm Compo: Si = 35.19%, O = 51.02%, Na = 9.81%, Ca = 2.16%, Al = 0.02%, K = 1.41% and Fe 0.39%

Figure 17: RBS Analysis for ANO annealed for 300°C for 1.45mins

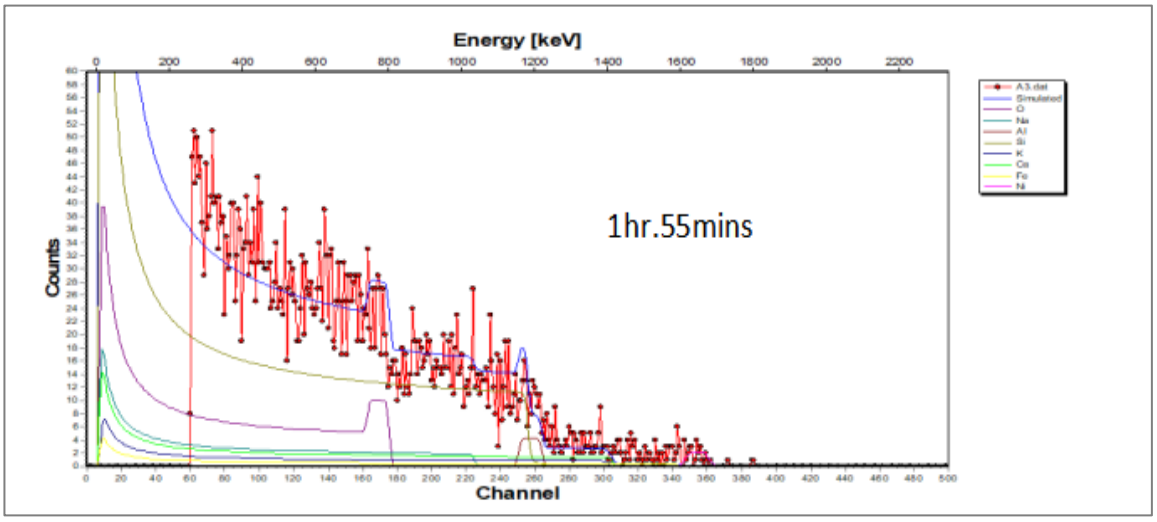

LAYER 1: THICKNESS: 223.0 nm Compo: Ni = 1.32%, Al = 15.14 %, O = 83.55%
LAYER 2: THICKNESS: 5000.0 nm Compo: Si = 35.19%, O = 51.02%, Na = 9.81%, Ca = 2.16%, Al = 0.02%, K = 1.41% and Fe = 0.39%

Figure 18: RBS Analysis for ANO annealed for 300°C for 1.55mins

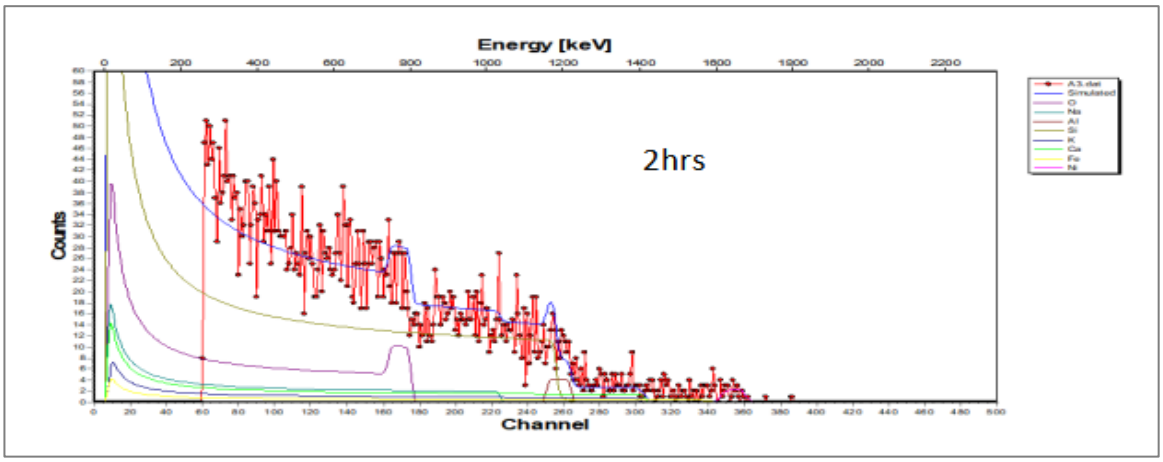

LAYER 1: THICKNESS: 350.0 nm Compo: Ni = 4.53%, Al = 13.28 %, O = 80.19%
LAYER 2: THICKNESS: 5000.0 nm Compo: Si = 35.19%, O = 51.02%, Na = 9.81%, Ca = 2.16%, Al = 0.02%, K = 1.41% and Fe = 0.39%

Figure 19: RBS Analysis for ANO annealed for 300°C for 2hrs

Table 2: Electric properties of ANO thin films annealed at varying time

Annealed time	Thickness (nm)	Resistance (Ω)	Sheet (Ω/sq.)	Resistivity (Ωm)	Conductivity (1/Ωm)
As grown	148	0.000281	0.001273	0.19	5.245
1.35 hrs.	150	0.000268	0.001212	0.37	2.661
1.45 hrs.	168	0.000200	0.000904	0.31	3.168
1.55 hrs	360	0.000180	0.000814	0.29	3.412
2.00 hrs	223	0.000150	0.000678	0.25	3.879

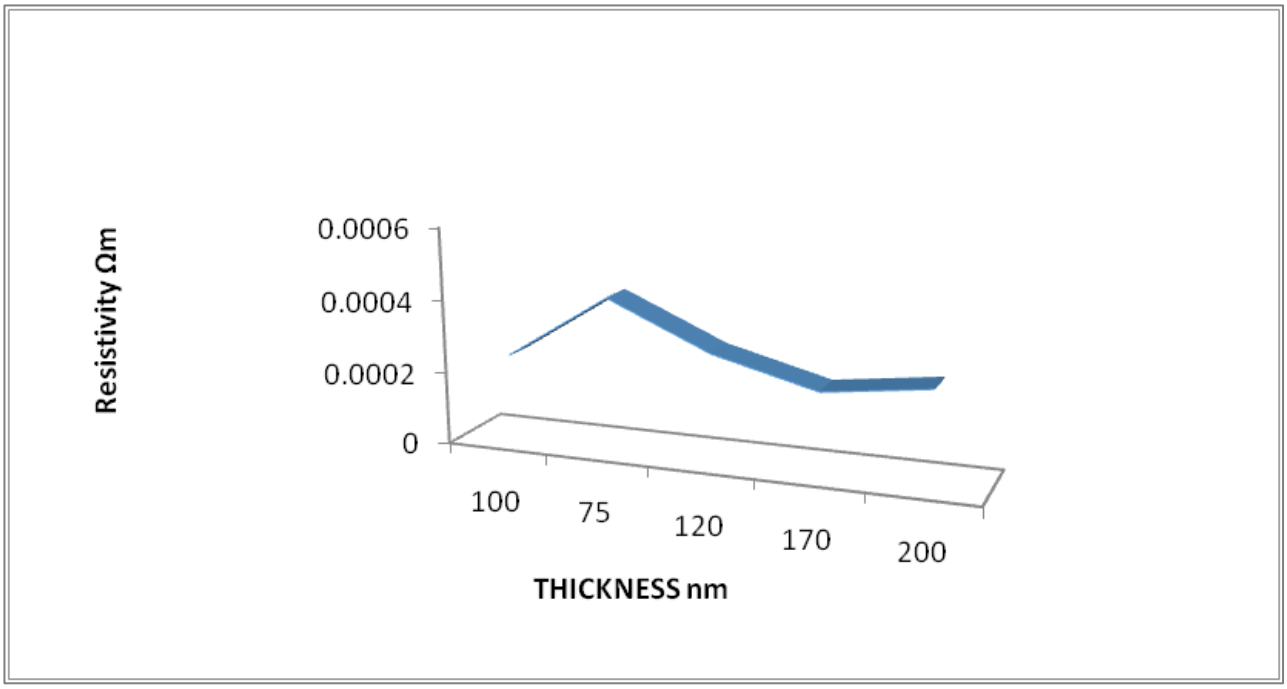

Figure 20: Plot of resistivity versus thickness for ANO thin films

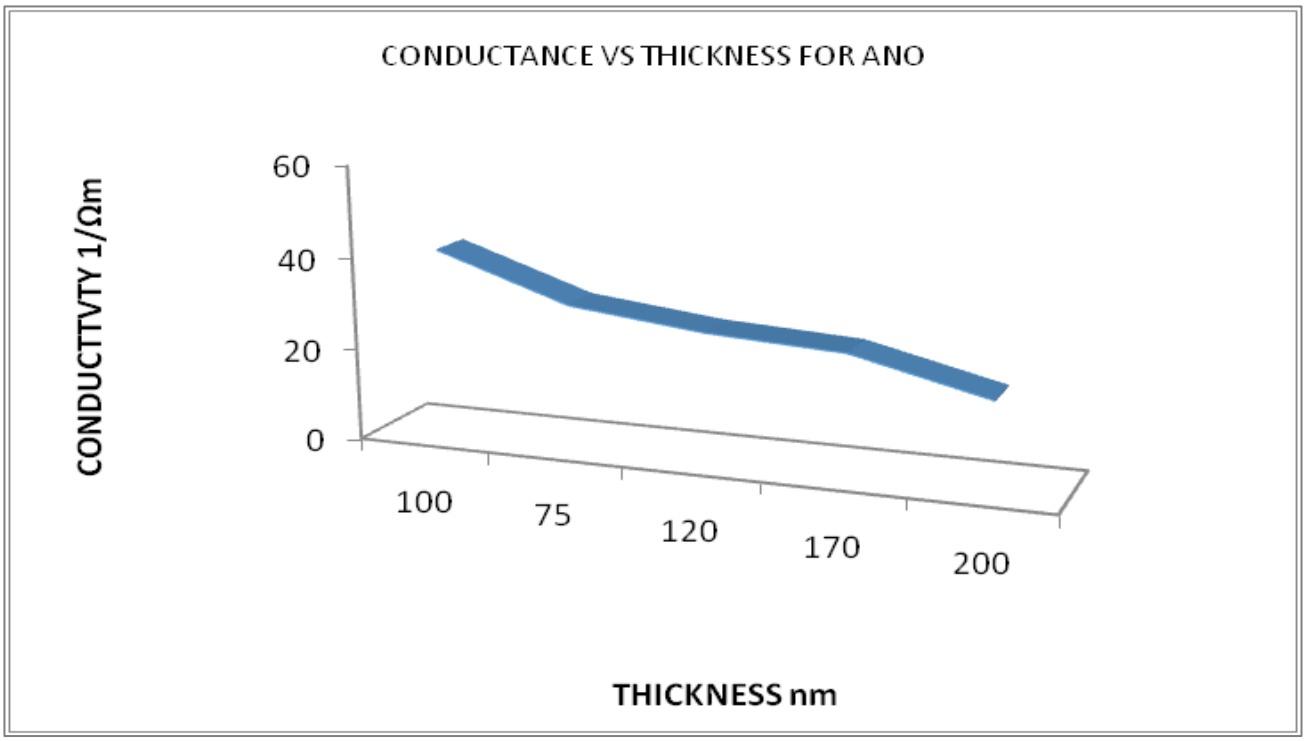

Figure 21: Plot of conductivity versus thickness for ANO thin films

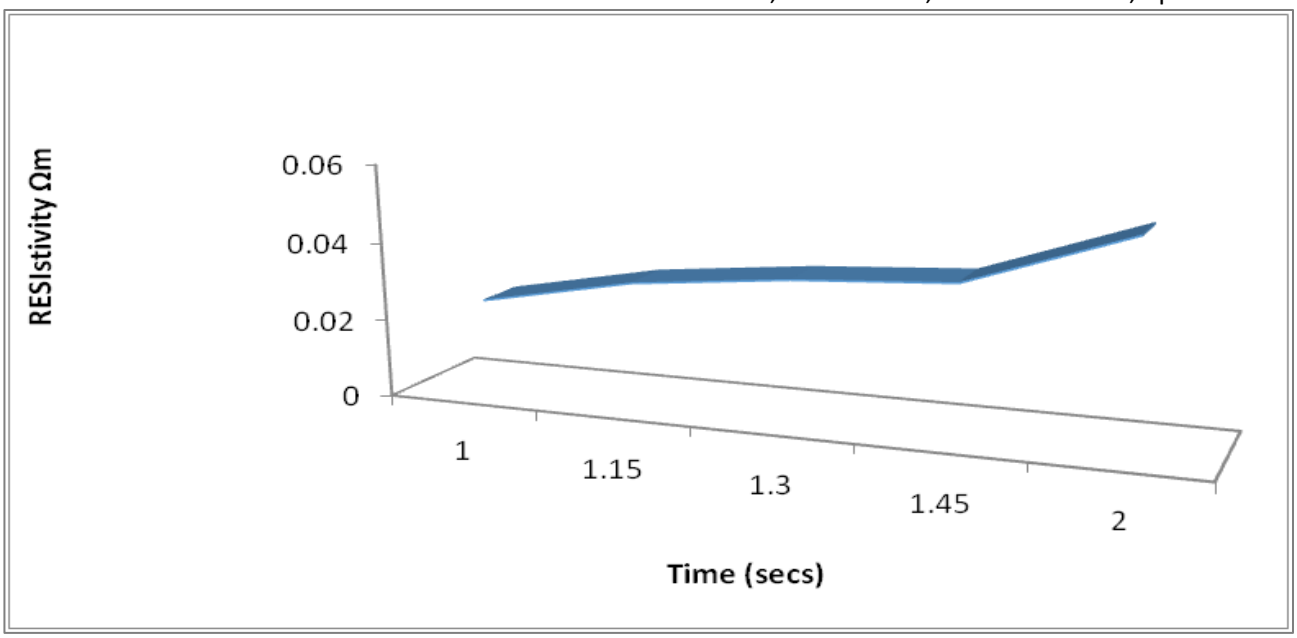

Figure 22: Plot of resistivity versus Annealing time for ANO films

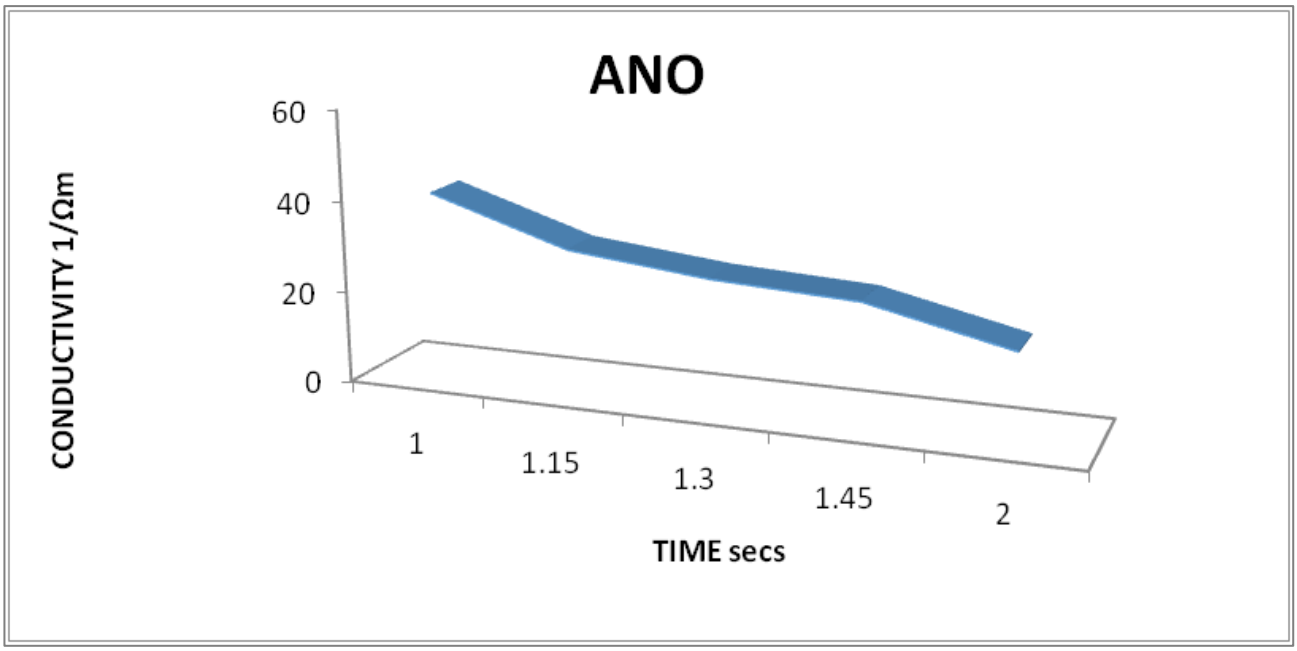

Figure 23: Plot of conductivity versus thickness for ANO thin films

CONCLUSION

NiO thin films doped with 10 % aluminum were deposited on a glass substrate using the SILAR method. The optical, structural, and electrical properties were studied. The films showed polycrystalline properties with a simple cubic phase of $NiAl_2O_4$ and a decrease in the crystallite size (2.228 µm – 0.1486 µm) as the annealing time increased from 1.35 hrs. to 2 hrs. The RBS showed that the film thickness increased with an increase in annealing time with a good percentage composition of Al, Ni, O. The electricity resistance was found to be low but increases with an increase in film thickness. The electrical conductivity was high and increased randomly with a decrease in thickness. The thin film material's good optical transparency, high electrical conductivity, and polycrystalline nature indicate their potential in optoelectronics devices, smart windows, and microelectronics. The low absorbances of the film indicate that the thin films may not be good materials for solar cell absorbers.

REFERENCES

Akpu, N.I., Asiegbu, A.D., Nnanna, L.A., (2022). Synthesis and characterization of novel yttrium-incorporated copper selenide (CuSe: Y) thin materials for solar energy applications. *J Material Science: Material Electron*33, 1154–1161. **[Crossref]**

Anusha,.S. Murthy .M., Sreelatha.C.J., (2023). Effect of Annealing Temperature Variation on Al-Doped Nickel Oxide Thin-Film Synthesized by Dip-Coating Technique. Solid State Phenomena. 350. 75-82. **[Crossref]**.

Boukhachem. A., Boughalmi. R., Karyaoui. M., Mhamdi .A., Chtourou.R., Boubaker ,K., Amlouk. M., (2014). Study of substrate temperature effects on structural, optical, mechanical and opto-thermal properties of NiO sprayed semiconductor thin films, Material Science Engineering. 188, 72–77. **[Crossref]**.

Ezeokoye, B. A. (2003). Optical properties of CUCL binary thin films deposited by solution growth method. *Greenwich Journal of Science and Technology*, 4(1): 365-368.

Gupta. N., Dileep. K., Mukul. G., Srihari. V., Choudhary. R. J., Rai. S. K., Pooja. G., (2022).Role of Nb content in tailoring the microstructure and magnetic anisotropy of soft magnetic W/CoFeB alloy thin films prepared with varying the substrate temperature, Journal of Alloys and Compounds, Volume 910,164930,ISSN 0925-8388. **[Crossref]**.

Haunsbhavi .K.,Kumar K.D.A.,Ubaidullah.M., Shaikh S.F., Venkatesh. R., Alagarasan. D., Angadi B., (2022). The effect of rare-earth element (Gd, Nd, La) doping of NiO films on UV photo detector, Physics Scripta 97 (5) 055815. **[Crossref]**.

Ibe, U. O and Mgbenu, E. N. (1997). Activation of annealing of Silver Films. *Nigerian Journal of Physics*, 9(4): 37-40.

Nid, A.; Zighed, L.; Aoun, Y.; Maaoui, B.,(2021)Synthesis and Characterization of Al-doped NiO Nanostructured Thin Films Elaborated by Solar Spray Pyrolysis Technique, for Photovoltaic Cells. 2021110572. **[Crossref]**

Mohammed A. H., Omar A. A., Sarmed S.M., Awadi A., (2020). Optical properties of Ag-doped nickel oxide thin films prepared by pulsed-laser deposition technique, *Optik*, Volume 206,2020,164352, ISSN 0030-4026. **[Crossref]**

Obaida, M., Fathi, A.M., Moussa, I. *et al.*(2022). Characterization and electro-chromic properties of NiO thin films prepared using a green aqueous solution by pulsed spray pyrolysis technique. *Journal of Materials Research* 37, 2282–2292. **[Crossref]**

Onwuemeka, J. J., Nwofor, O. K., Nwulu, N. C., Nwosu, E.I., Ezike, F. M., and Obizo, C. G., (2019). The Optical Study of ZnO Thin Films at Different Times of Annealing and Varying Temperatures. *Journal of Applied Physics (IOSR-JAP),* 6(1), 47-51.

Osuwa, J. C. and Uwaezi, U. P. (2012). Effects Annealing on the Optical, Structural and Electrical Properties of NiS^2 Thin Film.*Chalcogenide Letters*, 9(3),105-113

Osuwa, J. C. Ezema, F. I. and Oriaku, C. I. (2012). Laser induced Changes on Bend Gap and Optoelectronic Properties of Challogenide Glashy $CU_{0.11}$ $Cd_{0.40}S_{0.49}$ Thin Films. *Journal of Non Oxide Glasses*, 2(1): 1-5.

Pathan, H. M. and Lokhande, C. D. (2004). Chemical deposition and characterization of copper indium disulphide thin films. *Applied of Surface Science,* 239(1); 11-18.

Kumar. K., Saeed S.H., Pandey N.K, Verma V., Singh P., Yadav B.C., (2022). ,Influence of tin doping on the liquefied petroleum gas and humidity sensing properties of NiO nanoparticles,. *Journal of Material Resources* 37 (1) 369–379. **[Crossref]**.

Srinivasa N.V, Haunsbhavi .K, Srinatha .N., (2023). Preparation and characterization of Sn doped NiO thin films by sol–gel spin coating technique, *Materials Today: Proceedings* 5.597. **[Crossref]**

Tadatsugu, M., Yuki, N., Toshihiro, M. and Jun-ichi, N. (2016). High-Efficiency Oxide SolarCells with ZnO/Cu2O Heterojunction Fabricated on Thermally Oxidized Cu2O Sheets. *Applied Physics Express,*4, 062301.

Taeño .M, Maestre D., Ramírez-Castellanos J., Li S., Lee P.S, Cremades A., (2021). Towards control of the size, composition and surface area of NiO nanostructures by Sn doping, J. Nanomater 11 (2) 444. **[Crossref]**

Thi Ly Le. (2016). *Preparation of transition metal oxide thin films used as solar absorbers. Materials.*"Dissertation" Université Paul Sabatier - Toulouse III, English. <NNT : 2016TOU30120>. <tel-01578163>

Tuba .Ç.T, (2020). Synthesis of copper-doped nickel oxide thin films: Structural and optical studies, Chemical Physics Letters, Volume 738,136884, ISSN00092614. **[Crossref]**

Tlili .M., Nefzi .C., Alhalaili .B., Bouzidi .C, Ajili .L., Jebbari .N., Vidu .R., Turki Kamoun .N., (2021). Synthesis and Characterization of MgO Thin Films Obtained by Spray Technique for Optoelectronic Applications. *Nanomaterials.*;11(11):3076. **[Crossref]**

Yahya M. Abdul., Huda J. A., Latif L..A, Mudar A.A., Husham M. F.,(2019).Preparation of Al-doped NiO thin films by spray pyrolysis technique for CO gas sensing. Journal of Advance Pharmacy Education Research;9(3):1-6.

Yun A.J, Kim J. Hwang J., Park B., (2019). Origins of efficient perovskite solar cells with low-temperature processed SnO 2 electron transport layer, *ACS AppliedEnergy Material.* 2 (5) 3554–3560. **[Crossref]**

Zayim E.O, Turhan I., Tepehan.F.Z., Ozer .N., (2008) . Sol–gel deposited nickel oxide films for electro-chromic applications, Solar. Energy Material Solar Cells 92 (2) 164–169. **[Crossref]**.

Ugwu, Emeka & Onah, D.. (2007). Optical Characteristics of Chemical Bath Deposited CdS Thin Film Characteristics within UV, Visible, and NIR Radiation. Pacific Journal of science and Technology 8 (1)

Yang, Q., Hu, J., Fang, Y.-W., Jia, Y., Yang, R., Deng, S., Lu, Y., Dieguez, O., Fan, L., Zheng, D., Zhang, X., Dong, Y., Luo, Z., Wang, Z., Wang, H., Sui, M., Xing, X., Chen, J., Tian, J., & Zhang, L. (2023). Ferroelectricity in layered bismuth oxide down to 1 nanometer. Science, 379(6638), 1218–1224. **[Crossref]**